2-2022

Surface modified hybrid ZnSnO3 nanocubes for enhanced piezoelectric power generation and wireless sensory application

Sk Md Ali Zaker Shawon
The University of Texas Rio Grande Valley

Zaida D. Carballo
The University of Texas Rio Grande Valley

Valeria Suarez Vega
The University of Texas Rio Grande Valley

Chen Lin
The University of Texas Rio Grande Valley

Muhammad Sufian Rafaqut
The University of Texas Rio Grande Valley

See next page for additional authors

Recommended Citation

Shawon, Sk Md Ali Zaker, Zaida D. Carballo, Valeria Suarez Vega, Chen Lin, Muhammad Sufian Rafaqut, Andrew Xu Sun, J. James Li, and M. Jasim Uddin. 2022. "Surface Modified Hybrid ZnSnO3 Nanocubes for Enhanced Piezoelectric Power Generation and Wireless Sensory Application." Nano Energy 92 (February): 106653. https://doi.org/10.1016/j.nanoen.2021.106653

Surface modified hybrid $ZnSnO_3$ nanocubes for enhanced piezoelectric power generation and wireless sensory application.

Sk Md Ali Zaker Shawon[a], Zaida D. Carballo[b], Valeria Suarez Vega[a], Chen Lin[a], Muhammad Sufian Rafaqut[c], Andrew Xu Sun[a], James Li[d], M. Jasim Uddin [a*]

[a] *Department of Chemistry, Photonics and Energy Research Laboratory,* [b] *Department of Biomedical Sciences,* [c] *Department of Electrical Engineering,* [d] *DoD Consortium for Innovation Driven Research/Education Ecosystem for Advanced Manufacturing, University of Texas Rio Grande Valley, 1201 W. University Drive, Edinburg, TX-78539, USA,*

Corresponding Author Email: ***mohammed.uddin@utrgv.edu***

Abstract

Piezoelectric Nanogenerators (PENGs), which can convert ambient mechanical stimuli into electrical energy, are held in high regard due to their cost-effectiveness, energy harvesting applications, and potential as self-powered sensors. We report an aluminum-doped zinc stannate ($ZnSnO_3$) PENG that can achieve high electrical outputs with respect to the external force. In order to enrich the piezoelectric mechanics, a low-temperature solution method was adopted in our work to synthesize $ZnSnO_3$ nanocubes with an average side length of only 30 – 55 nm. Furthermore, $ZnSnO_3$ was doped with 1 wt% to 5 wt% of aluminum nanoparticles. We report that 2 wt% of aluminum doped $ZnSnO_3$ showed the highest electrical output in terms of open circuit voltages and short circuit current. The nanogenerator device achieved an average open-circuit voltage of 80 V to 175 V with a frequency range of 60 BPM (Beats Per Minute) to 240 BPM, an unprecedented electrical output in comparison to current $ZnSnO_3$-based PENGs. With the presented high output-to-size ratio taken into consideration, the device was mounted in a helmet and tested as an energy harvester and wireless human motion sensor, which can generate electric charge as well as detect human movements and transmit the corresponding signals wirelessly. Our work- is indicative of a promising smart helmet using organic-inorganic hybrid materials.

Keywords: Piezoelectric Nanogenerator, Renewable Energy, Sensors, Smart Helmet.

Graphical Abstract:

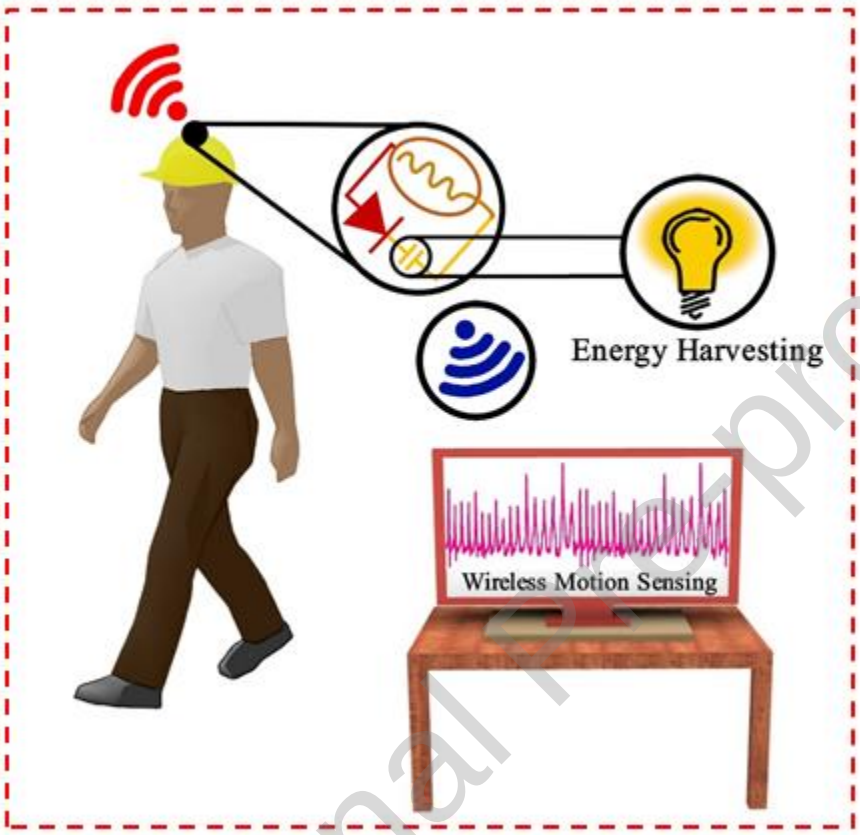

1. Introduction

In recent years, research on acquiring energy from innovative sources has accelerated, motivated by an increasing desire to address the energy crisis and demand for wireless, portable electronic devices [1-4]. Widely available in the environment, ambient energy, can come in the form of mechanical, thermal, or solar energy. These sources have spiked interest in the scientific community [5-7]. Various devices have been fabricated to take advantage of the energy existing all around us; solar cells, electrostatic generators, pyroelectric nanogenerators, electromagnetic generators are just a few [4, 8-11]. Among these devices, piezoelectric nanogenerators (PENGs), which can convert mechanical vibrations (e.g., biological movement, acoustic noise, low-frequency vibrations, airflow, etc.) into electrical energy are promising candidates for energy

harvesting due to their versatility [12-16]. Additionally, they have many prospective applications such as in healthcare, self-powered sensing, wearable, and implantable devices, etc. [12, 17-20].

The first PENG was fabricated using ZnO nanowires in 2006 [21], and since then, ZnO-based nanogenerators have continued to be a focus in research and innovation due to their low cost, varied possible morphologies, and good piezoelectric properties [22, 23]. However, even as the output has been improved considerably over the years (from 9 mV to ~200V), it is still insufficient to fully power portable devices [24, 25]. Meanwhile, the potential of other materials in energy harvesting has also been explored, including PZT which garnered attention for its high piezoelectric coefficient. However, its low conductivity and biological incompatibility impedes its output and limits its implantable or wearable applications, respectively; its lead component is also toxic [26]. Another example is a flexible HPNG consisting of PVDF and AlO-rGO by integrating steel woven fabric electrodes. This HPNG showed an open circuit output voltage of 36V, a current of 0.8 μA and a power density of about 28 μW cm^{-3} under repeating finger tapping [27].

On the other hand, the burgeoning admiration for lead-free perovskite oxides as piezoelectric energy harvester have drawn attention of the scientific community owing to their non-toxic tradeoff for piezoelectric output, as well as chemical and structural stability[28, 29]. For example, in 2017, Baek et. al. synthesized $BaZr_xTi_{1-x}O_3$ nanoparticles and adopted this material in a flexible piezoelectric energy harvester; with Zr concentration of 32 mol%, the resulted device generated a stable output voltage about 20 V and a current signal of 400 nA [30]. Also, a recently published review summarized general approaches and recent progresses in synthesis, and related energy harvesting devices [31].

In this regard, $ZnSnO_3$- a multifunctional semiconductor, shows promise in the field of energy harvesting. Its high remnant polarization (P_r = 59 μC/cm^2) along the c-axis is conducive to higher output performance. Additionally, unlike many piezoelectric ceramics, which require electrical poling to align crystal orientations [24], $ZnSnO_3$ exhibits self-poling behavior under mechanical strain, facilitating easy nanogenerator fabrication [32, 33]. The carbon-thermal reaction, hydrothermal, coprecipitation, low-temperature ion exchange methods have all been used to create $ZnSnO_3$ crystallites [32, 34]. However, since the material can present various

morphologies and structures and easily decomposes above 750 ℃, a suitable synthesis method is vital to obtain $ZnSnO_3$ with excellent energy-harvesting characteristics. Presently, $ZnSnO_3$ nanowires[35], microbelts [36, 37], nanorods [38], nanoplates [39], and nanocube [32, 40-42] have been used in energy harvesting. The nanocube morphology is one of the most common. Aqueous sol-gel techniques have been used for the synthesis of metal oxide nanoparticles. However, the resulting precipitates are often amorphous, and need an extra annealing step which leads to particle growth. Hydrothermal synthesis needs high temperatures and long synthesis periods. The cubic zinc stannate morphology can be obtained by low temperature ion exchange, which allows for small particles with a larger surface area.[43] These characteristics are desirable for higher outputs in PENGs. The larger surface area allows for higher sensitivity of the $ZnSnO_3$ sensor. [32, 42].

However, the electric output level of PENGs is still one of their greatest limitations. Many output enhancing methods have focused on suppressing the free carrier screening effect, by which free carriers diminish the piezopotential caused when a piezoelectric material is strained [36]. For example, the effects of doping, surface modifications, and particle treatment on the screening effect have all been investigated [44-46]. In terms of the enhancement of $ZnSnO_3$-based nanogenerators, Paria *et al.* recently added a CuO layer to their PENG, forming a p–n heterojunction to screen for electrons [47]. Alternatively, other techniques include the use of MWCNT to allow for a more uniform distribution of $ZnSnO_3$ in polydimethylsiloxane (PDMS) [33] and microstructuration to facilitate the distribution of force that can be converted into electrical energy [48]. However, doping has been investigated for other semiconductors but it has never been used for $ZnSnO_3$-based PENGs to enhance output by altering the crystal structure of $ZnSnO_3$ [49].

Herein, we present a novel technique to enhance the efficiency of a $ZnSnO_3$PDMS piezoelectric nanogenerator by doping $ZnSnO_3$ with aluminum nanoparticles. $ZnSnO_3$ nanocubes were synthesized using the low temperature solution method, allowing for the deliberate formation of small particles sizes (average of 30 – 55 nm). The synthesis of $ZnSnO_3$ nanocubes with the particle size range of 30 nm to 55 nm in nanogenerators is also unprecedented. Furthermore, Aluminum oxide (Al_2O_3) was added in varying amounts to accomplish Al nanoparticle doping into the ZnSnO3 structure. The ionic radius of Al^{3+} is close to the radius of both of Zn^{2+} and

Sn^{4+}. Thus, aluminum doping plays a key role in decreasing the lattice parameters, and the resulting distortion contributes to the enhanced piezopotential, producing significantly higher electrical output without any poling operation.[50] Experiments conducted using the range of 1% (w/w) to 5% (w/w) of Al nanoparticle doped in $ZnSnO_3$ nanocubes, among which 2 wt% Al doped $ZnSnO_3$ exhibited the highest piezoelectricity. The doped $ZnSnO_3$ nanocubes were dispersed into PDMS to create the piezoelectric film, which retained its functional properties while enhancing the physical and chemical stability of the nanocubes [51]. The device achieved an average open circuit voltage of 80 V to 175 V under a finger-tapping load frequency of 60 BPM (60 BPM, 120 BPM, 180 BMP, and 240 BPM is equivalent to 1 Hz, 2 Hz, 3 Hz, and 4 Hz respectively) to 240 BPM. The maximum short circuit current was found to be 20 µA with a power density range of 600 mW/m^2 to 2900 mW/m^2. Under finger tapping conditions, enough energy was produced to lit 28 LEDs, showing the device's potential to convert ambient mechanical energy and power portable devices. Additionally, it has applications in self-powered sensing, the PENG was incorporated into a helmet to detect impact and motion. In this work, we have demonstrated the application of the as-synthesized piezoelectric film by incorporating it into a helmet capable of detecting human motion while walking and running. A circuit comprised of microprocessors was also designed to show the wireless motion sensing capability of this Al doped $ZnSnO_3$ PENG.

2. Experimental

2.1 Synthesis of Zinc Stannate ($ZnSnO_3$) Nanocubes

All the chemicals were of analytical grade from Sigma Aldrich and used without further purification. The low-temperature solution method was used to synthesize the $ZnSnO_3$ nanocubes [52]. 20 mmol of both $ZnSO_4 \cdot 7H_2O$ and $Na_2SnO_3 \cdot 3H_2O$ were each dissolved in 100 ml DI water, making two solutions. The former was placed in an ice bath to maintain the temperature at 1 °C while the second solution was added dropwise. The reaction for the $ZnSnO_3$ synthesis is shown by equations 1 and 2. The 1:1 molar ratio mixture was allowed to react at a temperature of 1°C for 12 hours after the solution was centrifuged (Fisher HealthCare© Horizon

Model 614B) and washed with ethanol and DI water to remove any residual ions. The centrifuged product was placed in a (Ney© Vulcan 3-1750) oven to dry for 12 hours at 110 °C. The experimental procedure concluded with $ZnSnO_3$ nanocubes with an average particle size of 30-55 nm.

Equation 1. $ZnSnO_3$ formation reaction.

$$ZnSO_4 \bullet 7\,H_2O + Na_2SnO_3 \bullet 3\,H_2O \xrightarrow[1\,℃]{DI\ H_2O} ZnSnO_3$$

Equation 2. Ion exchange reaction for $ZnSnO_3$ synthesis.

$$Zn^{2+} + {SnO_3}^{2-} \xrightarrow[1\,℃]{DI\ H_2O} ZnSnO_3$$

2.2 Doping of Aluminum in Zinc Stannate

Aluminum oxide (Al_2O_3) mesoporous particles (3.5 nm) were dispersed in a $ZnSnO_3$-ethanol mixture. The mixture was then placed in an oven for evaporating and drying for 12 hours at 120 °C. The dried mixed powder was mortared and pestled for 1 hour to ensure uniform mixing before being placed in the furnace for 8 hours at 600 °C for calcination. The calcined Al-doped $ZnSnO_3$ powder was washed thoroughly with DI water, and ethanol and then centrifuged to remove any unwanted impurities. After that, the as synthesized powder was again dried in an oven for 12 hours at 120 °C.

2.3 Nanogenerator Fabrication

To prepare the Aluminum-doped $ZnSnO_3$ piezoelectric film, Polydimethylsiloxane (PDMS), Ethyl acetate, and a curing agent were combined in a ratio of 10:6:1 and vigorously stirred. Subsequently, 20 wt% of the compounded Aluminum-doped $ZnSnO_3$ powder was added to the PDMS solution and stirred for 3 hours to uniformly disperse it. The resulting solution was placed into a Petri dish, vacuumed for 1 hour to remove air pockets, and dried in an oven for 5 hours at 120 °C, forming the piezoelectric film of an effective area of 12.25 cm^2 with a film thickness of

~1mm. After being bilaterally attached to two pieces of copper tape and wire, the film and electrodes were encapsulated (to enhance durability) with PDMS solution composed of PDMS, ethyl acetate, and a curing agent in a 10:1:2 ratio. The encapsulated film was dried in an oven (Ney© Vulcan 3-1750) in 3 intervals: 1 hour at 60 °C, 1 hour at 100 °C, and 2 hours at 120 °C. The morphological characterization and electrical characterization are discussed broadly in the supporting information (S.1 and S.2).

3. Results and Discussion

It has been reported that optimized distribution of dopants parallel to the [0 0 1] direction in ABO_3 type perovskite systems contributes to the enhanced piezoelectric potential of the perovskite system [50]. In our work, during the calcination of Al doped $ZnSnO_3$ powder at 600 ˚C, Al^{3+} ion diffuses into the lattice parameter of $ZnSnO_3$, thus causing a distortion of the $ZnSnO_3$ structure. The Al^{3+} substitution at the A-site can increase the doping level of Sn^{4+} at the B-site, maximizing the distortion upon mechanical stress. The ionic radius of Al^{3+} (0.62 A˚) is close to the ionic radius of Zn^{2+} (0.88 A˚) and Sn^{4+} (0.83 A˚). Thus, the larger mismatch of the A-site cation to the B-site cation plays a key role in decreasing the lattice parameters, and the resulting distortion of the crystal structure contributed to the enhanced piezopotential; producing significantly higher electrical output without any kind of poling operation. Besides, with the smaller cubic crystal size of $ZnSnO_3$, it possesses a higher surface area, and uniform distribution of mechanical stress induces greater distortion of lattice parameters which results in additional electrical output.

Moreover, the Al-doped $ZnSnO_3$ nanocubes are dispersed into the PDMS maintaining 20 wt% concentration of Al-doped $ZnSnO_3$ was demonstrated to be the most optimum ratio for maximizing the piezoelectric output by previous studies [26, 32]. In addition to that, the piezoelectric material to PDMS weight ratio of 20:100 is reported to be the most optimum recipe for the uniform distribution of the piezoelectric material into the PDMS matrix [53-55]. Increase in Al-doped $ZnSnO_3$ concentration into the PDMS matrix results in high piezoelectric potential which is attributed to the resultant higher dielectric constant. On the other hand, increasing the Al-doped $ZnSnO_3$ concentration might cause weak insulation of the

nanocomposite leading to electrical breakdown. So, in our study, we have used 20 wt% concentration to achieve the most possible aligned electric dipoles of Al-doped $ZnSnO_3$ into the PDMS matrix.

Figure 3.1 illustrates the structure and working mechanism of the PENG. The as-fabricated Al-doped $ZnSnO_3$ – PDMS film as shown in Figure 3.1(a), was sandwiched between two layers of thin copper tape attached to copper wires, which served as the electrodes to conduct the electrons from the film. Together, these pieces formed the functional component of the PENG as shown in Figure 3.1 (b). Next, the film and electrodes were encapsulated with PDMS to enhance the device's durability against various environmental conditions and direct impacts. The device can be seen in Figure 3.1(c) in comparison to the size of a hand.

The working mechanism of the device can be understood by looking at the effect of a mechanical load on the Al-doped $ZnSnO_3$ nanocubes. At first, the ions within each nanocube are uniformly distributed. When an external force is applied, such as the pressure from a finger, the compression of the $ZnSnO_3$ structure creates a piezopotential from the polarization of its ions, as seen in Figure 3.1 (d). This polarization can be attributed to $ZnSnO_3$'s non-centrosymmetric structure [56]. The compression shifts the relative positions of cations and anions and creates a dipole moment. Simultaneously, the resulting dipoles of each nanocube unidirectionally align with each other, accumulating a significant potential difference between the top and bottom electrodes.

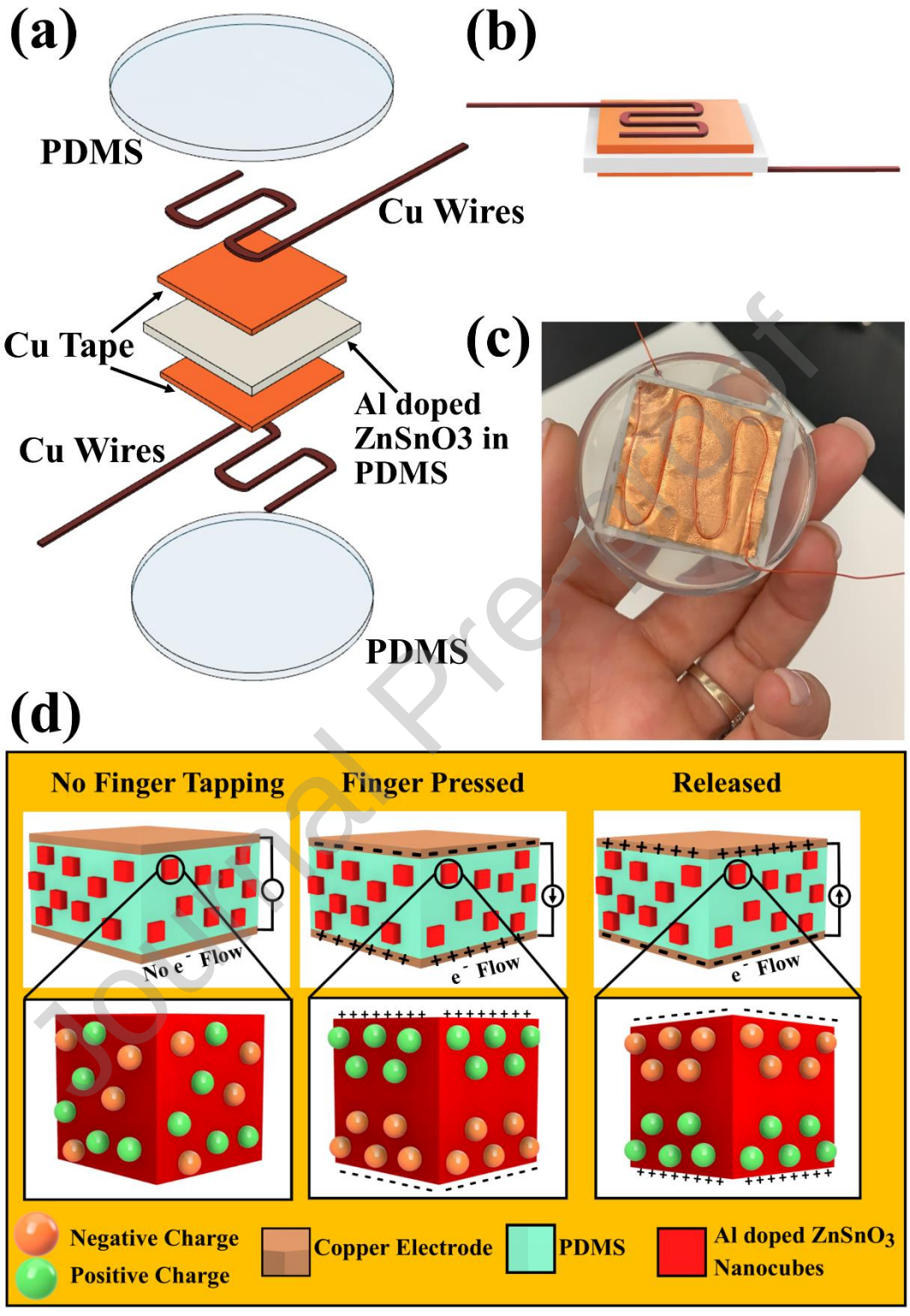

Figure 3.1: Detailed schematic of the (a) encapsulated Al doped $ZnSnO_3$ piezoelectric film and (b) the Al doped $ZnSnO_3$ piezoelectric film with electrodes. (c) Size of the film compared to a hand. (d) Schematic diagram of the working mechanism of the film.

Thus, when the two electrodes are connected in a closed circuit, electrons flow from the negatively charged electrode to the positively charged one in an attempt to balance the charge, similar to the current flow which results from a charged capacitor [57]. When the force is released, the ions within each nanocube briefly invert before returning to their original distribution. Since electrons had once flowed to the positive electrode, that electrode now becomes negatively charged from the excess of electrons as the electric dipoles no longer align to sustain their original positive charge. There is a flow of electrons in the opposite direction compared to when the PENG was compressed. Thus, continuous compression and release create an alternating electrical current, which can then be converted into direct current with consistent voltage using a bridge rectifier and capacitor [58].

The morphology of synthesized samples was examined by SEM. Figure 3.2-(a), (b), and (c) show the SEM images of undoped $ZnSnO_3$, and (d), (e), and (f) are images for $ZnSnO_3$ doped with 2% (w/w) of Al nanoparticles. Formed particles are round-corner cubes, in the nanometer range. The size of the particles composed of undoped $ZnSnO_3$ is in the range of 35–50 nm, while for the doped sample, the size ranges between 30–55 nm. After Al doping, the size distribution of the nanomaterial increases, which significantly contributes to the electrical output properties of the doped $ZnSnO_3$ piezoelectric film.

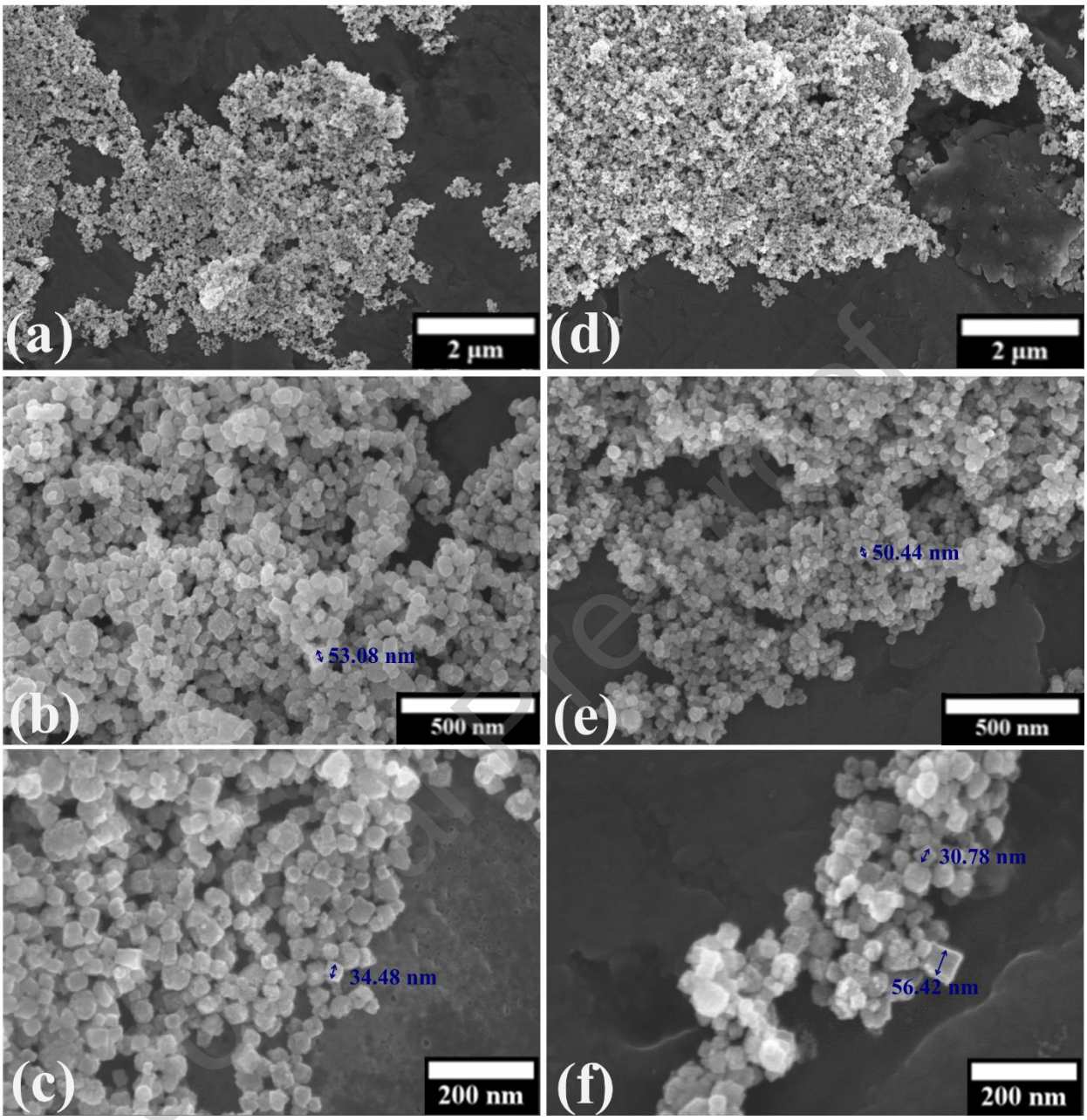

Figure 3.2: SEM images of undoped $ZnSnO_3$ (a,b,c) and $ZnSnO_3$ doped with 2% (w/w) of Al nanoparticles (d,e,f).

In Figure 3.3 (a) the SEM image was used to obtain EDX spectrum and elemental mapping images. The EDX spectrum in Fig. 3.3(b) shows all the elements, i.e., O, Zn, Al, and Sn. Zn and Sn occupying L-shells were found at 1.01 and 3.44 eV, respectively. O and Al occupying K-shells were observed at 0.52 and 1.49 eV, respectively. The inset of Figure 3.2 (b) shows the

table with the weight and atomic percentages of the elements present. The weight percent of Al is 1.90%. EDX spectrum and the inset table prove the successful doping of Al in $ZnSnO_3$. Fig. 3.3 (c) to 3.3 (f) show the elemental mapping images which indicate the uniform distribution of these elements. EDX results of the 2 wt% sample is reported here, as this doping level gives the best piezoelectric performance. Besides, the same experimental procedures are adopted to prepare all samples with different doping levels. Under the same experimental conditions, doping was successful, and the actual weight percentage of doped Al in samples should be very close to the indicated value (1%, 3%, 4%, and 5%). To support the claim of uniform distribution of all the components in the synthesized powder; the highest dopant concentration (5 wt% Al doped) $ZnSnO_3$ EDX mapping is added in the supporting information (Figure S7).

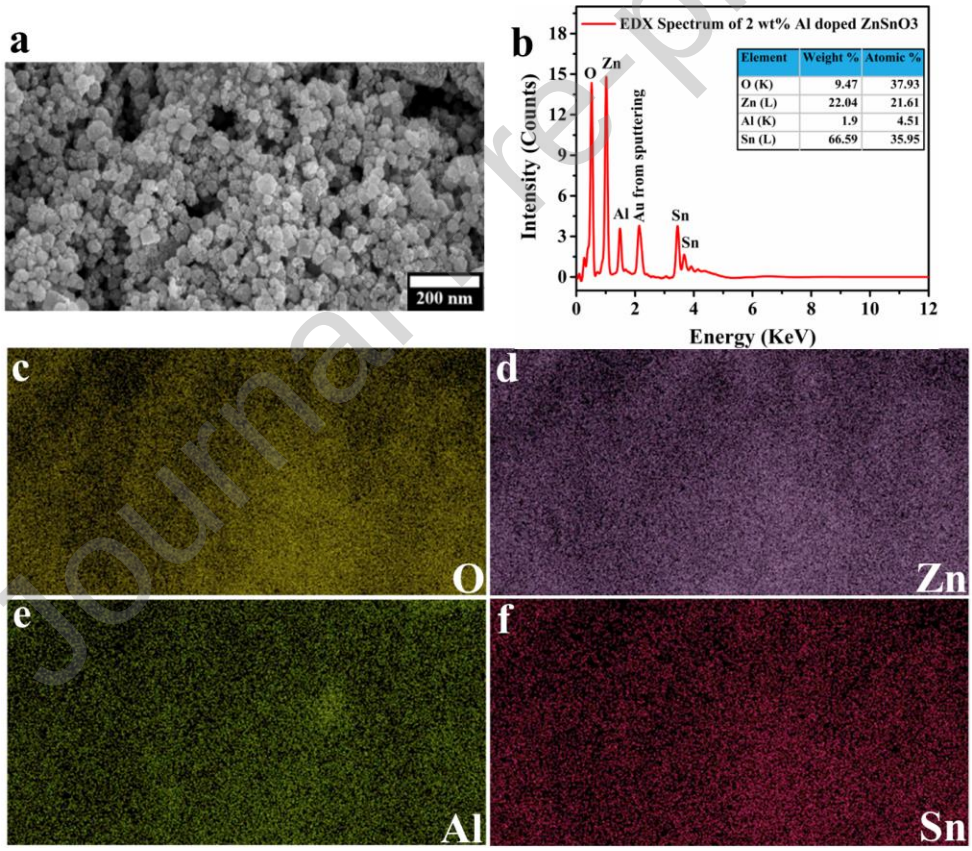

Figure 3.3: (a) SEM image, (b) EDX spectrum, (c) to (f) elemental mapping images of O, Zn, Al, and Sn, respectively.

The XPS analysis is a useful tool to study structure and surface chemical compositions. Figure 3.4 shows the survey scan XPS spectrum of $ZnSnO_3$ doped with 2% Al (w/w), and the one below has high-resolution spectra of the individual elements, i.e., Zn, Sn, O, and Al (Figure 3.4- (b) to (e), respectively). Binding Energy (BE) in the survey scan spectrum has the range of 0–1300 eV and reveals all the elements. The peak with a BE value 284.11 eV is assigned to C, and the source of C in the sample is CO_2 in the air. The Al 2p peak has very low intensity, especially when comparing with Sn, Zn, and O peaks. The Sn 3d peak can be resolved into two peaks, i.e., Sn $3d_{5/2}$ at 486.97 eV and Sn $3d_{3/2}$ at 495.45 eV, which correspond to Sn in the sample. In the spectrum, we also observed Sn 4d, Sn $3p_{3/2}$, and Sn $3p_{1/2}$ signals at 28.15, 718.16, and 760.03 eV, respectively, which are due to different Sn orbitals in the sample. Note that in high-resolution spectra for Zn and Sn showed in the figure below, all peaks are deconvoluted into a single peak. A single component for each peak suggests that almost all Zn and Sn in the sample have the same oxidation states, i. e., Zn has oxidation state +2, and Sn has oxidation state +4, throughout the whole sample. The asymmetric O 1s can be split into two peaks. The peaks were observed at the BE values of 532.22 eV and 530.82 eV related to the oxygen atoms in the form of Sn–O–Sn and Zn–O–Sn, respectively. Therefore, the XPS result confirms the uniformity of the sample.

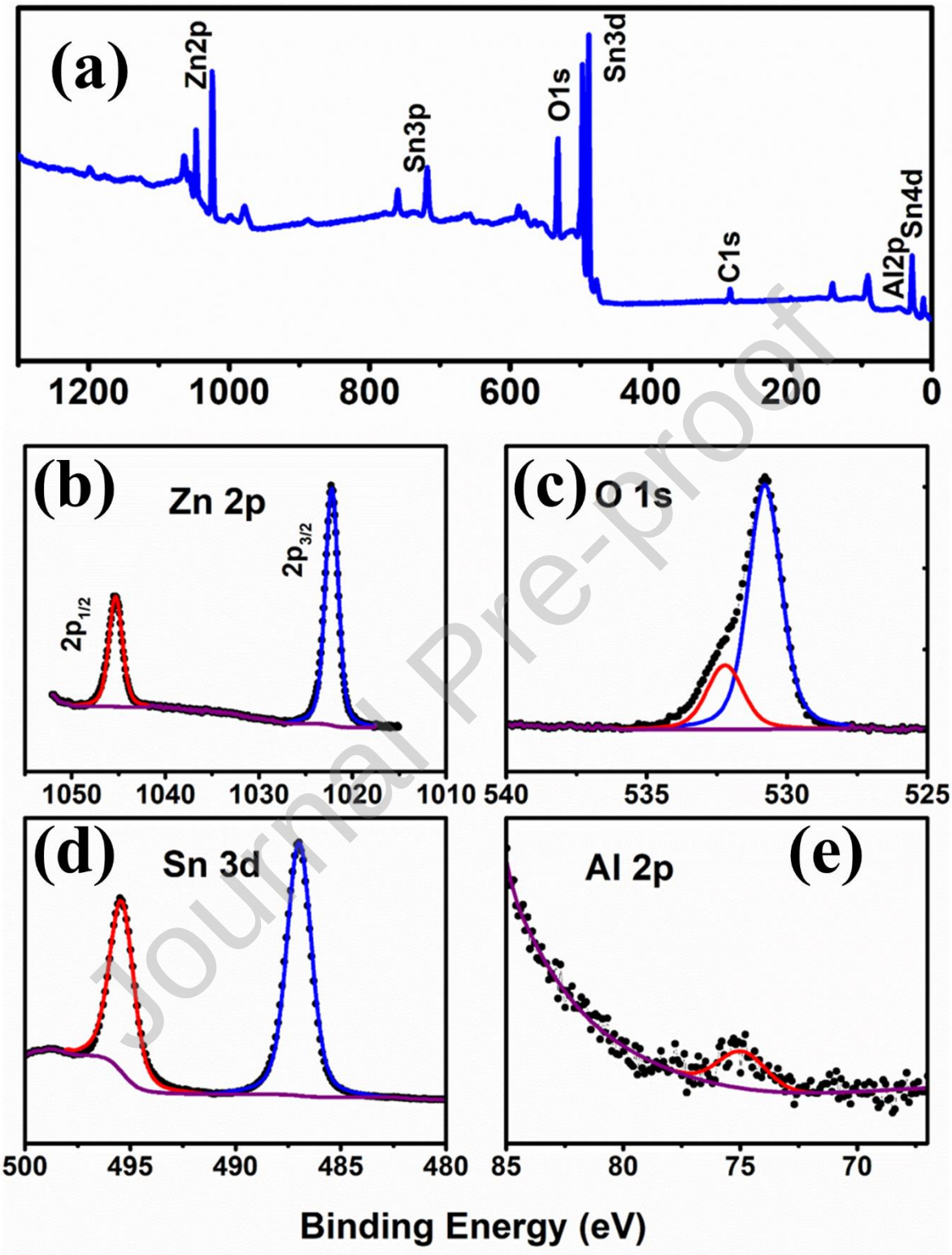

Figure 3.4: (a) Shows the survey scan XPS spectrum of $ZnSnO_3$ doped with 2% Al (w/w), and the high-resolution spectra of the individual elements, i.e., (b) Zn, (c) O, (d) Sn, and (e) Al.

Figure 3.5 shows the XRD patterns of undoped and doped $ZnSnO_3$. Black lines in the Figure show the XRD patterns of undoped $ZnSnO_3$. The sample shows XRD spectrums with very similar peaks that can be successfully assigned to $ZnSnO_3 \cdot 4H_2O$. However, after doping, the major component becomes tetragonal SnO_2 (2%, 3%, and 4% samples) or cubic Zn_2SnO_4 (1% and 5% samples). For 2%, 3%, and 4% samples, peaks that appear at 2θ = 26.3°, 33.6°, 51.5°, 65.1°, 71.2°, and 83.4° correspond to the (110), (101), (211), (112), (202), and (222) crystal planes of tetragonal SnO_2, respectively. In the case of 1% and 5% samples, signals at 2θ = 34.3°, 41.7°, 51.7°, 55.1°, and 60.4° correspond to the (311), (400), (422), (511), and (440) crystal planes of cubic Zn_2SnO_4, respectively. From 2% sample to 4% sample, when Al doping percentage is increased, the intensity of XRD peak at 26.3° for the tetragonal SnO_2 (110) plane decreases. This might suggest a possible doping position of Al in the crystal structure. In spectra for 3% and 4% samples, the appearance of peak labeled with ♦ suggests the existence of cubic $ZnAl_2O_4$, which indicates the doping of Al into crystal structures. In addition, the peak labeled with * at 41.0° could be assigned to monoclinic $Al(OH)_3$, and the peak labeled with ▼ may be due to hexagonal Zn. Samples with 1% and 5% doping show the conversion from $ZnSnO_3 \cdot 4H_2O$ to Zn_2SnO_4.

The intrinsic electronic structure of $ZnSnO_3$ has favored its enhanced piezoelectric potential compared to the other ABO_3 type perovskites [28]. When the lower valent ion (A) in the ABO_3 type perovskite is Zn^{2+}; it gives rise to a 3D electronic structure owing to the formation of Zn-O_6 covalent bonds. This 3D electronic framework results in enhanced charge distribution followed by higher carrier mobility and a decrease in the bandgap [59, 60]. In addition to this, the SnO_6-ZnO_6 octahedral framework in $ZnSnO_3$ causes the semiconducting oxide behavior of this species. The significantly low resistivity (4×10^{-3} Ω cm), and higher electrical charge mobility of $ZnSnO_3$ are attributed as the function of its 3D octahedral structure, shows enhanced piezoelectric potential and structural stability [61-63]. Doping of $ZnSnO_3$ with various concentrations of Al mesoporous particles to achieve non-centrosymmetry coupled with higher piezoelectric potential have essentially increased the total piezoelectric output in our synthesized PENG.

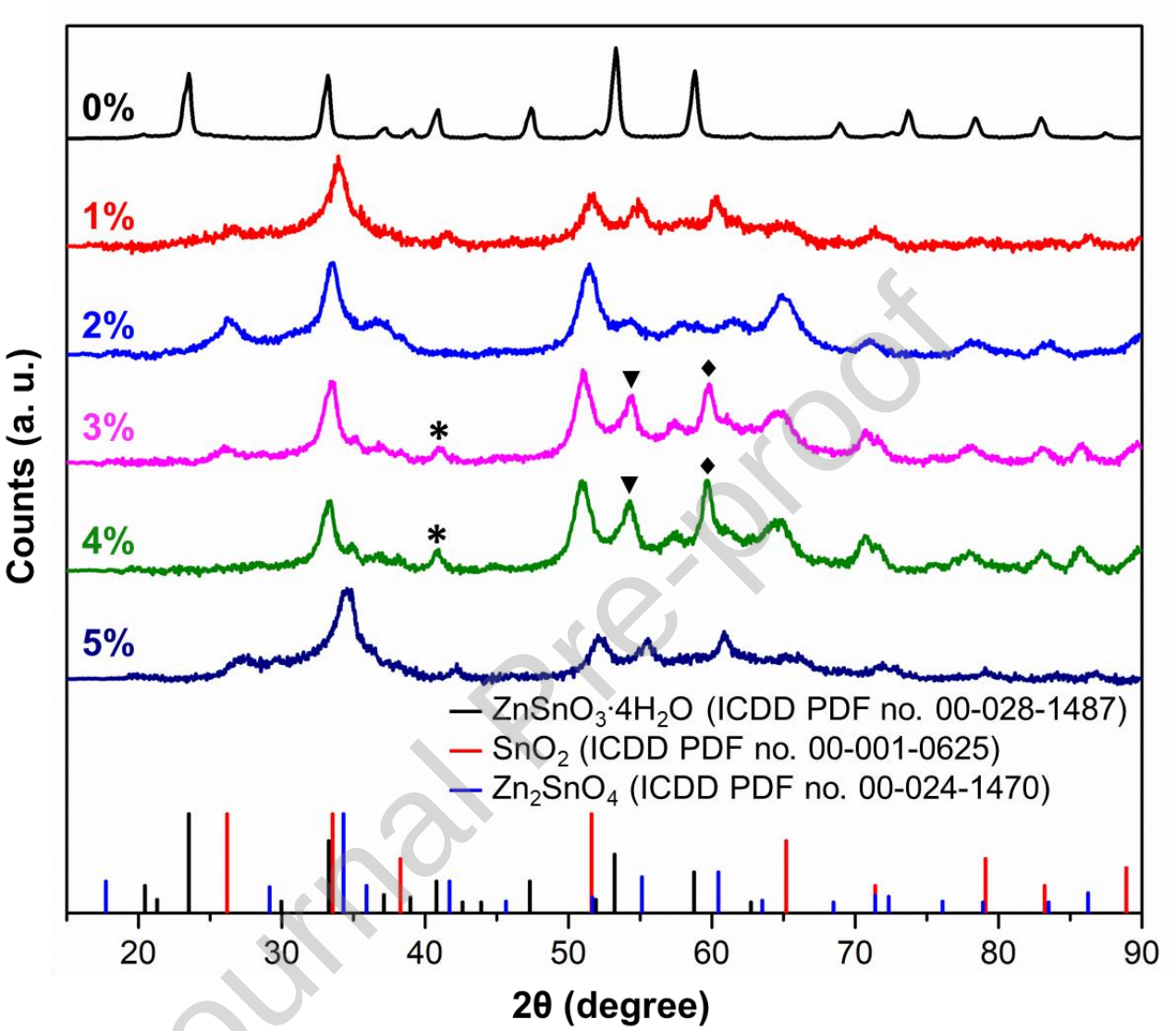

Figure 3.5: XRD patterns of Al-doped $ZnSnO_3$ powders. XRD peak positions for $ZnSnO_3{\cdot}4H_2O$, SnO_2, and Zn_2SnO_4 are also present for comparison. Peaks labeled by different symbols are: (*) $Al(OH)_3$ (monoclinic, ICDD PDF no. 00-077-0177), (▼) Zn (hexagonal, ICDD PDF no. 00-001-1244), and (♦) $ZnAl_2O_4$ (cubic, ICDD PDF no. 00-073-1961)

The investigation of Al doping on the piezoelectric properties of $ZnSnO_3$ was done through the output testing of several PENGs. This work focuses on the influence of Al doping to enhance the piezoelectric output of unpoled $ZnSnO_3$ and the significant output change of the doped samples

over undoped ones are carefully reported. By only varying, the dopant concentration in the functional piezoelectric material from 0 wt% (undoped) to 5 wt%; this work has presented the significant influence of Al doping on $ZnSnO_3$ in terms of various electrical outputs (V_{OC}, I_{SC}, and power density).

The piezoelectric output of our PENG is recorded by varying the finger tapping frequency from 60 BPM to 240 BPM (60 BPM = 1 Hz, 120 BPM= 2 Hz, 180 BPM= 3 Hz, 240 BPM= 4 Hz; here BPM stands for Beats Per Minute) and approximate finger tapping force applied is ~0.2 N. Data obtained for various frequencies and applied force on different Al dopant concentration of $ZnSnO_3$. With the increasing finger tapping frequency and applied force on each dopant concentration; the piezoelectric output increases which is supported by the literature and discussed widely in our previous works[6, 16, 64-66]. Here in Figure 3.6 (a) shows the results for the time-dependent open circuit voltage (V_{OC}) at a finger tapping load frequency of 120 BPM. Similar data has been acquired for various finger tappings load frequencies, such as 60 BPM, 180 BPM, and 240 BPM. The results are enlisted in supporting information (Figure S1 to S3 in S.I). With no aluminum doping (0 wt% Al), the Al doped $ZnSnO_3$ PENG achieved a positive V_{OC} of ~50V, which steadily increased to ~90V and ~110V at 1 wt% and 2 wt% of Al, respectively. Thus, Al doping of $ZnSnO_3$ can markedly improve the V_{OC} of the PENG, at least in smaller concentrations. Indeed, from 3 wt% and onwards, the output began decreasing at each concentration, from ~70V to ~60V; 5 wt%, the voltage was ~40V, which was even lower than the pristine $ZnSnO_3$ nanogenerator.

However, the addition of Al must be carefully measured as excessive amounts are detrimental to performance. Overall, the largest increase in voltage occurred in that initial 1 wt% addition of Al, but it eventually began tapering and decreasing when more dopant was added until the treatment became disadvantageous. Significant effects of the dopant wt% on maximizing the output and the PENGs output limited by an optimal wt% of the dopant concentration is customarily reported in various works [67-72]. This paper proposes that the cause of the decrease in output as Al doping concentration increased beyond 2 wt% can be attributed to the oversaturation of Al^{+3} at the A-site (Zn) of ABO_3 ($ZnSnO_3$) type perovskite systems. As explained earlier, up until 2 wt%, the addition of Al dopants modifies the crystalline structure of $ZnSnO_3$ such that there is

greater distortion and charge separation upon mechanical pressure. However, beyond that point, it follows that additional Al doping into $ZnSnO_3$ lattice leads to an excess of cations which can no longer be incorporated in the crystal lattice, instead precipitating out. As Al_2O_3 itself has no piezoelectric properties, its presence in excess begins interfering with the distortion upon stress of the piezoelectric material. Thus, charge generation and output are hampered.

Note that, in this study, the 5 wt% sample has a very similar XRD pattern to the 1wt% sample (Figure 3.5), while the piezoelectric performance is the lowest among all doping levels. A possible explanation is that XRD signals are not monotonic functions of doping level. 1% doping of Al changed hydrated $ZnSnO_3$ into Zn_2SnO_4, while higher doping levels (2% to 4%) facilitates the formation of SnO_2 and Al-containing structures. However, 5 wt% of Al might be too high, so that hydrated $ZnSnO_3$ can only change into Zn_2SnO_4, while the excess of Al compared to 1% sample greatly suppressed the piezoelectric performance of the device. Further study is needed to investigate this phenomenon.

Figure 3.6 (b, c) shows that the short circuit current (I_{SC}) and power density followed this general trend as well. For the 2wt% Al-doped PENG, the short circuit current of ~13 μA. I_{SC} at various finger tapping frequencies (60 BPM, 180 BPM, 240 BPM) are also recorded and have been enlisted in the S.I (Figure S4 to Figure S6).

When comparing the output power densities, it was found that the 2 wt% Al dopant concentration provides a power density of ~1200 mW/m^2, which was about four times greater than the undoped PENG at ~300 mW/m^2. This relationship is consistent with the previous result of roughly a two-fold increase for both voltage and current. The high-power output of the PENG shows its feasibility as a miniature, portable power source. As discussed earlier, the dopant contributes to the higher piezoelectric potential which attributes to the higher dielectric constant. Al doping in $ZnSnO_3$ modifies the crystalline structure, such that—greater distortion and charge separation is ensured upon mechanical stress. But Al itself does not have any piezoelectric properties, so beyond a certain concentration of Al dopant, increasing the dopant concentration further directly interferes with the crystal distortion of $ZnSnO_3$ upon any mechanical stimuli, resulting in a significant decrease in the piezoelectric

output. For our case, that optimal concentration threshold is 2 wt% of Al in $ZnSnO_3$, as at this concentration the PENG harvested maximum piezoelectric output and shows detrimental effect in terms of electrical output when the dopant concentration is further increased.

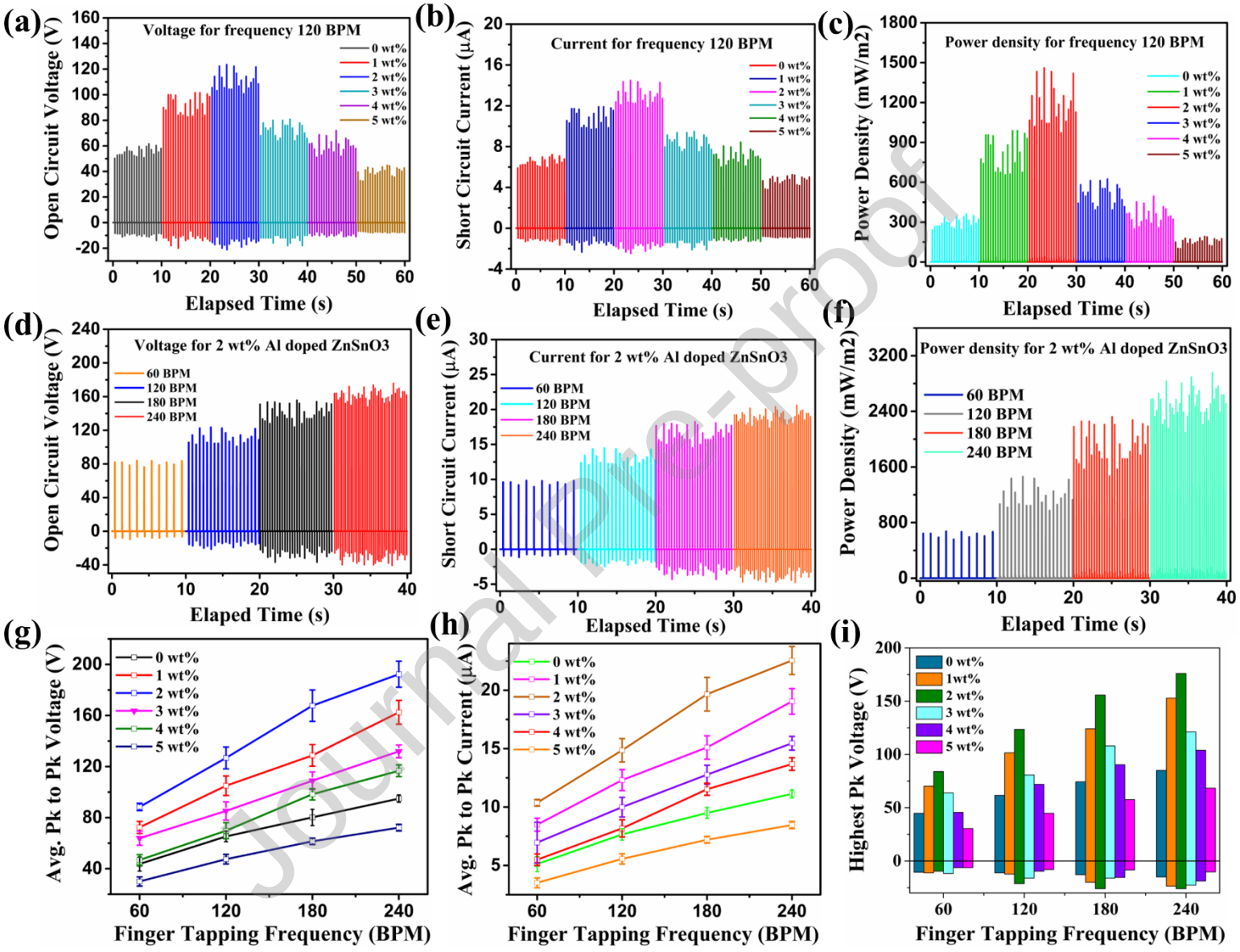

Figure 3.6: (a) The open circuit voltages, (b) short circuit currents, and (c) power density of PENGs with various concentrations of Al doping in $ZnSnO_3$. (d) The open circuit voltages, (e) short circuit currents, and (f) power density for a PENG doped with 2 wt% aluminum at various finger tapping frequencies. (g) The average peak to peak voltages, and (h) currents for all ranges

of Al doping Concentration in $ZnSnO_3$ at various finger tapping frequencies. (i) The Peak voltages for all ranges of Al doping Concentration in $ZnSnO_3$ at various frequencies.

Additionally, the output performance of 2 wt% Al doped $ZnSnO_3$ PENG was further evaluated for different finger-tapping frequencies. As seen in figure 3.6 (d), starting at a rate of 60 BPM, the PENG produced a positive open circuit voltage of ~80V which steadily increased to ~100V, ~130V, and ~170V with every additional 60 BPM. For this reason, comparing the effect of Al dopant concentration on output performance required that the frequency of mechanical disturbance be held constant, preventing it from skewing the results. Figure 3.6 (e, f) shows that I_{sc} and power density also increased approximately linearly with higher frequencies, starting with an output of ~10 μA at 60 BPM and reaching ~18 μA at 240BPM. The overall increase in output is consistent with previous literature and can be attributed to a decrease in impedance caused by the higher tapping frequency, which leads to better impedance matching and power transfer [73-76]. The ability of the most optimally Al doped PENG to generate considerable electrical output at a variety of frequencies demonstrates its feasibility in applications involving the ambient environment, where the available mechanical disturbances in the ambient environment are likely to be unpredictable. The high output of the PENG can be reasonably attributed just to the piezoelectric effect rather than a hybrid of piezoelectric and triboelectric: The device's configuration insulates triboelectric charges from the output. Meanwhile, the charge on the PDMS would not likely have substantially impacted the output due to PDMS's charge insulating properties combined with its thickness in our nanogenerator (thickness of the device after encapsulation ~ 1cm). Indeed, for many PDMS-based triboelectric nanogenerators, the thickness of PDMS is only about 0.5 mm or less [77-80].

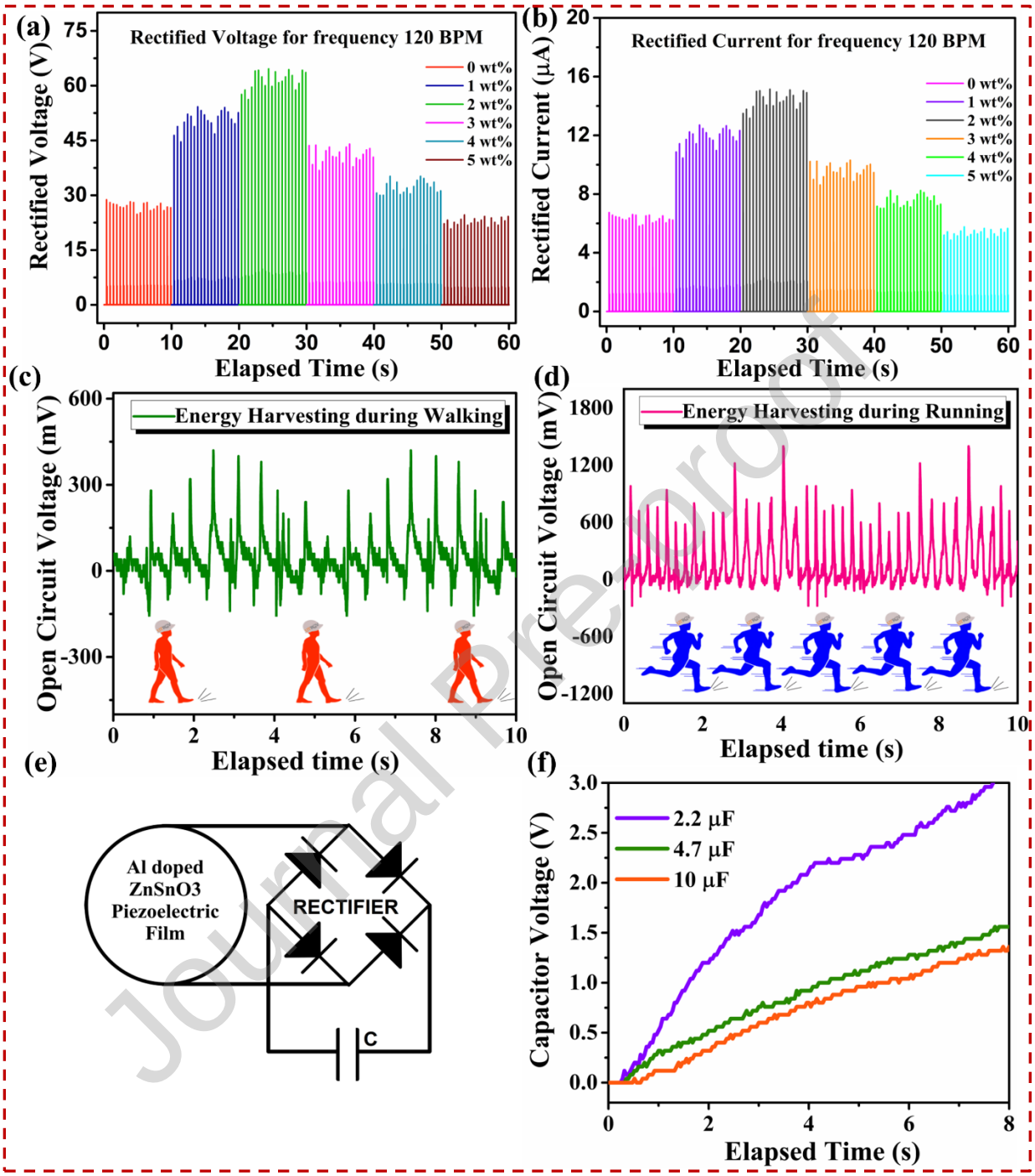

Figure 3.7: (a) Rectified voltage, and (b) current for all the doping concentrations at the finger tapping frequency of 120 BPM. (c) The open circuit voltages during walking, and (d) running with the smart helmet. (e) Circuit diagram of the Al doped $ZnSnO_3$ PENG connected to a rectifier to charge a capacitor. (f) The voltage levels of a 2.2 μF, 4.7 μF, and 10 μF capacitor in respect to the time for which the PENG charges them at a random finger tapping frequency.

Each wt% of Al doped PENG responds similarly in terms of output when the frequency is increased. The impact of both the wt% of Al dopant and the frequency of finger tapping on the peak-to-peak voltage (V_{Pk-Pk}) and current (I_{Pk-Pk}) is summarized in Figure 3.6 (g, h). The 2 wt% Al doped PENG had the highest average V_{Pk-Pk} and I_{Pk-Pk}, which was approximately double that of the pristine PENG at nearly every frequency. The lowest performance was at 5 wt% Al doping. Additionally, from 60 to 240 BPM, a 4-fold increase, the output average $V_{Pk-Pk,}$ and I_{Pk-Pk} roughly doubled. Figure 3.6 (i) illustrates the highest peak voltages from each wt% Al doped PENG at every frequency, the absolute highest voltage recorded being 176 V.

The PENG's feasibility as a portable power source and energy harvester was also evaluated. To make the output from the PENG more useful for that purpose, the alternating current was rectified to a direct current, which is more appropriate to power electronic devices. As seen in Figure 3.7 (a) and (b) the rectified voltage and current of the device declined compared to the AC voltage and current. The rectified voltage and current probed simultaneously, which results in a similar trend in response to the tapping output. In Figure 3.6 (a) and (b) due to a dissipation of energy occurring as the current passes through the diodes and the rectifier. The use and development of higher-efficiency rectifiers could help mitigate this issue [81].

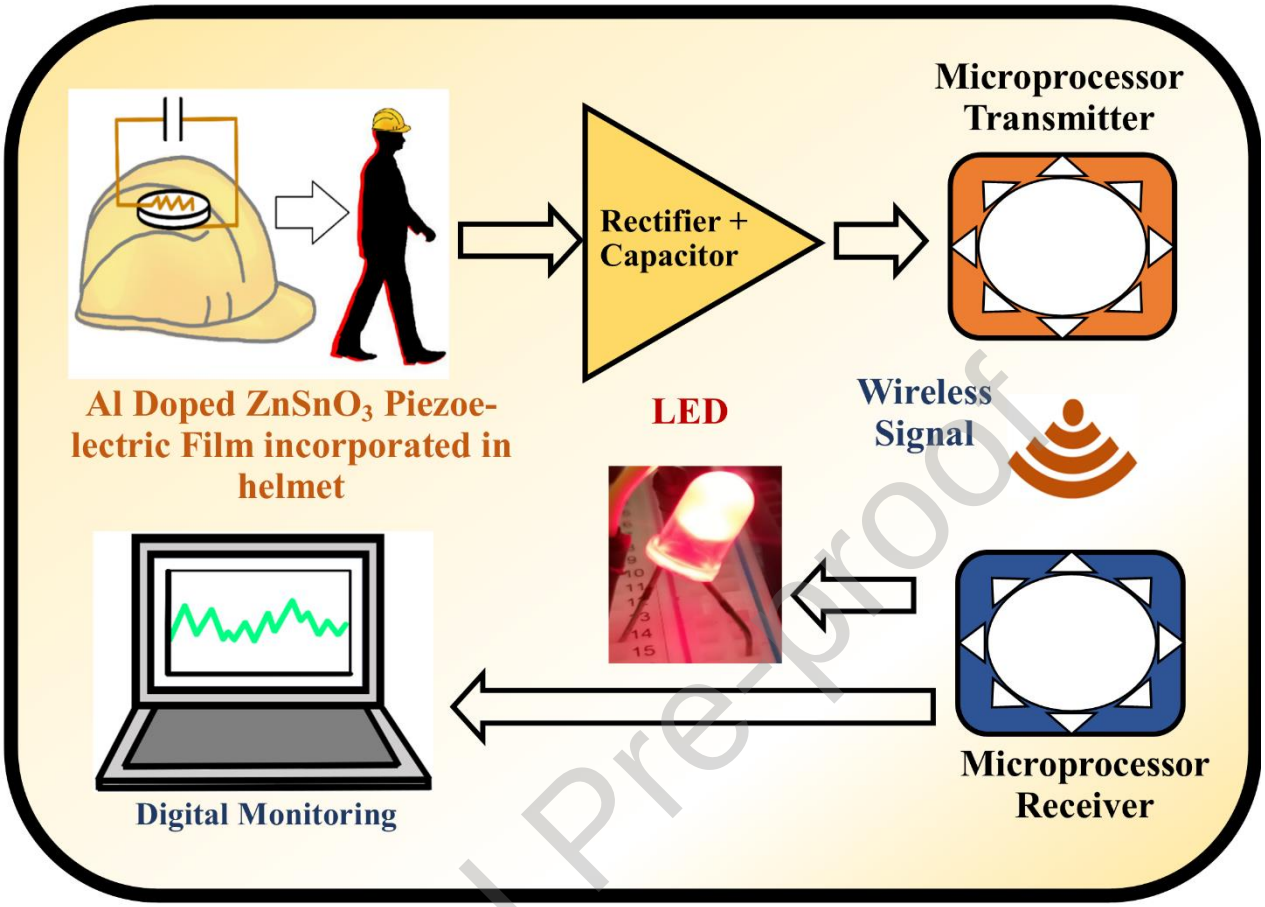

Figure 3.8: A schematic diagram for a motion-sensing system using the PENG.

The PENG was installed inside of a helmet to allow the device to seamlessly convert the energy from human motion, namely walking and running. The arrangement demonstrates one way in which the PENG can be used as an energy harvester. In Figure 3.7 (c), the output of the device reached up to 400 mV when walking, being compressed from the momentum of each step. The output from minute compression during random walking and running clearly indicates the high size to response ratio of the device. The details of the helmet's energy harvesting feature can be also demonstrated from the video attached in the supporting information (Video-2). In this case, the value of the PENG lies in its ability to steadily capture energy unobtrusively and over an extended period. In contrast, when the wearer of the helmet was running in Figure 3.7 (d), the peak voltage reaches ~1200 mV, as the compressions on the device increased in frequency. The increase in electrical output while running due to higher frequency compression and relaxation of

the device into the helmet can be referred to a similar explanation as for the higher outputs obtained for finger tapping and has been already discussed in the prior sections.

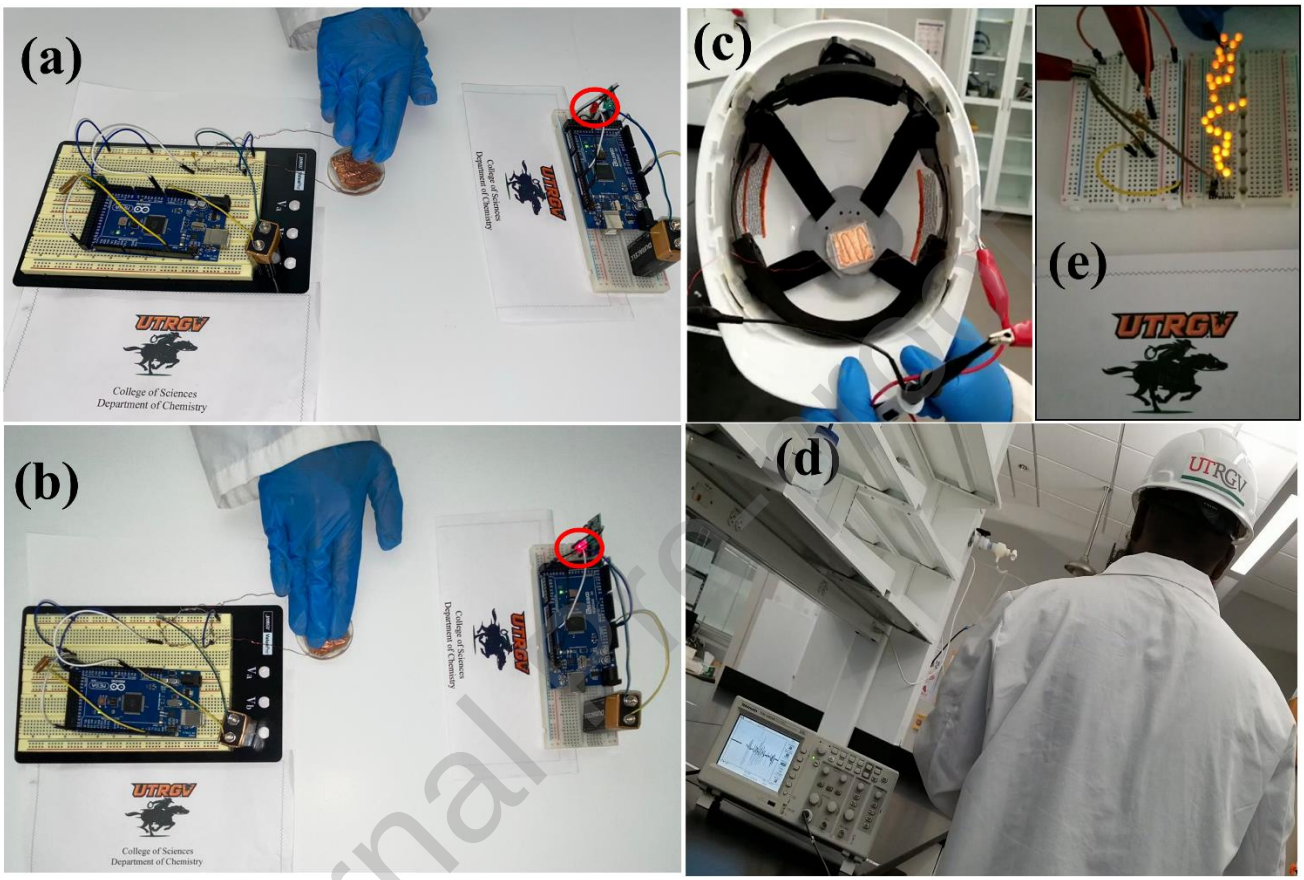

Figure 3.9: Wireless signal generation testing upon compression of fingers. (a) LED is not lit as the fingers weren't touching with the Al doped PENG, (b) LED is lit upon finger tapping. (c) A helmet with Al doped $ZnSnO_3$ piezoelectric film incorporated, and (d) motion (Walking and Running) detection in terms of open circuit voltage with an oscilloscope using the helmet-PENG arrangement. (e) Random finger tapping of the Al doped $ZnSnO_3$ piezoelectric film harvests energy to light 28 LEDs.

Interestingly, the unique patterns of voltage peaks from Figure 3.7 (c, and d) also demonstrate that the PENG can be used as a self-powered motion sensor. Both the frequency of steps and the relative magnitude of the footstep force can be indicated. The output of a PENG, especially harvesting energy from the environment, can be inconsistent. A way to store the energy

generated is important for their practical application (supporting information, Video-2). Figure 3.7 (e) shows one arrangement in which the PENG is connected to a bridge rectifier and capacitor. The charging of a capacitor voltage: when charged by a PENG under finger-tapping is illustrated in Figure 3.7 (f). The device was capable of charging capacitors. Tested with 3 capacitors it showed to reach output capacitance-voltage of 3V for 2.2 μF in only 8 seconds. At this same time, capacitance voltage reaches ~1.5V and ~1.0V for the case of capacitors with a capacitance range of 4.7 μF and 10.0 μF respectively. Thus, our PENG device is evaluated based on a number of electrical parameters (Open circuit voltage, short circuit Current, Pk-Pk voltages, Capacitance voltage, Rectified voltages and Current, and Power). Evaluating our PENG based on these parameters significantly validates the comparison of this device with other works in this same field. Also this approach of evaluating the PENG based on these parameters completely aligns with our previous works [6, 16, 64-66].

In addition to its energy harvesting capacities, the Al doped $ZnSnO_3$ nanogenerator can also be used in sensory applications, particularly for detecting the motion of any nature. This function is due to its ability to spontaneously respond to mechanical stress with electrical output. The lack of requirement for a battery or other external power source bestows the device's advantages over other sensors that are power-dependent. For example, our PENG can continuously operate for longer and is more compact. One such motion sensing system to detect human gait is illustrated in Figure 3.8, the PENG is attached to the top part inside of a helmet, with its AC signal passed through a rectifier to convert it into a rectified DC signal. The PENG sensors are placed parallel to the rectifier and capacitor, read the voltage, and send it to a microprocessor (MP), which sends a wireless signal through a radio frequency (RF) transmitter. After reaching the RF receiver paired with another MP, the wireless signal prompts that MP to turn on an LED, indicating that the PENG is generating voltage (supporting information, Video-3). The information can be displayed in two ways: dichotomously (i.e., with the LED light, ‘on’ for motion and ‘off’ for motionless) or continuously (having the generated signal being displayed on a computer screen). Figure 3.9 (a-e) is a physical representation of the idea presented in Figure 3.8, where finger tapping on the PENG connected to a transmitter wirelessly turns on an LED connected to a receiver acting as a switch. Of course, as soon as there is no compression on the PENG, the LED turns off. Figure 3.9 (c) shows the PENG being attached to a helmet, and the unit was worn on

the head and tested to detect walking. As shown in Figure 3.9 (d), the voltage generated by the PENG can be recorded wirelessly. The electrical output of the PENG was able to be displayed on Tektronix TDS 1001B oscilloscope when the helmet and PENG device were worn while walking, The PENG demonstrated its output capabilities by lighting 28 LEDs with only finger tapping as seen in Figure 3.9 (e). The sensitivity of the device, the large voltage to input ratio, and wireless signal transmission, demonstrate the ability of the Al doped $ZnSnO_3$ PENG to be used as a human motion sensor. This work also suggests further studies on the future improvements in the PENGs sector. Even the implementation of self-healing noncentrosymmetric molecular crystals can be studied in the future for new PENGs [82].

4. Conclusion

The future utilization of PENGs and sustainable energy share a conjoined prospect of success. To recapitulate, we have proposed a novel method for the fabrication of a high-output PENG that comprised a composite of Al-doped $ZnSnO_3$ nanocubes and PDMS. The enhanced output can be attributed to the modified $ZnSnO_3$'s crystalline structure, the introduction of aluminum cations modified and the reduced size of $ZnSnO_3$ nanocube particles synthesized through the low-temperature solution method. It was found that a 2 wt% Al-dopant concentration was most optimal; the resulting PENG generated an electrical output of ~110 V, 13 μA, and 1200 mW/m2 under only 120 BPM (2 Hz) finger-tapping input. This conversion efficiency is, to our best knowledge, unprecedented for a $ZnSnO_3$-based nanogenerator. The high output-to-input ratio suggests that the PENG has high potential in both scope and practicality for energy harvesting and sensory applications. The Al-doped $ZnSnO_3$ PENG could charge a 2.2 μF capacitor to 3V in only 8 seconds with finger tapping. This paper proposes a system in which the PENG can act as a motion sensor through its integration inside a helmet. The device generated electricity corresponding to each of the wearer's footsteps, which was converted into a wireless signal to detect human mechanical movement. Overall, the Al-doped $ZnSnO_3$ PENG has a high value in converting and detecting ambient mechanical energy. However, more investigation on specific applications and systems that can efficiently transfer the energy generated is still needed to realize further utilization.

Declaration of Competing Interest

The authors declare that they have no known competing financial interests or personal relationships that could have appeared to influence the work reported in this paper.

Acknowledgments

Sk Md Ali Zaker Shawon and Valeria Suarez Vega acknowledge the Graduate College of the University of Texas Rio Grande Valley for the Presidential Graduate Research Assistantship. This work was supported by the U.S. Department of Defense Manufacturing Engineering Education Program (MEEP) program under Award No. N00014–19-1–2728.

References:

[1] M.J. Alam, S.M.A.Z. Shawon, M. Sultana, M.W. Rahman, M.M.R. Khan, Kinetic study of biodiesel production from soybean oil, 2014 POWER AND ENERGY SYSTEMS: TOWARDS SUSTAINABLE ENERGY, IEEE, 2014, pp. 1-5.
[2] Z.L. Wang, Self - powered nanosensors and nanosystems, Wiley Online Library, 2012.
[3] G. Zhu, Z.-H. Lin, Q. Jing, P. Bai, C. Pan, Y. Yang, Y. Zhou, Z.L. Wang, Toward large-scale energy harvesting by a nanoparticle-enhanced triboelectric nanogenerator, Nano letters 13(2) (2013) 847-853.
[4] S.K. Karan, S. Maiti, J.H. Lee, Y.K. Mishra, B.B. Khatua, J.K. Kim, Recent Advances in Self-Powered Tribo-/Piezoelectric Energy Harvesters: All-In-One Package for Future Smart Technologies, Advanced Functional Materials 30(48) (2020) 2004446.
[5] F. Yildiz, Potential Ambient Energy-Harvesting Sources and Techniques, Journal of technology Studies 35(1) (2009) 40-48.
[6] E. Islam, A.M. Abdullah, A.R. Chowdhury, F. Tasnim, M. Martinez, C. Olivares, K. Lozano, M.J. Uddin, Electromagnetic-triboelectric-hybrid energy tile for biomechanical green energy harvesting, Nano Energy 77 (2020) 105250.
[7] B.D. Choudhury, C. Lin, S.M.A.Z. Shawon, J. Soliz-Martinez, J. Gutierrez, M.N. Huda, F. Cesano, K. Lozano, J.Z. Zhang, M.J. Uddin, Carbon Fibers Coated with Ternary Ni–Co–Se Alloy Particles as a Low-Cost Counter Electrode for Flexible Dye Sensitized Solar Cells, ACS Applied Energy Materials 4(1) (2021) 870-878.
[8] B.D. Choudhury, C. Lin, S.M.A.Z. Shawon, J. Soliz-Martinez, H. Huq, M.J. Uddin, A photoanode with hierarchical nanoforest TiO 2 structure and silver plasmonic nanoparticles for flexible dye sensitized solar cell, Scientific reports 11(1) (2021) 1-11.
[9] R. Tashiro, N. Kabei, K. Katayama, Y. Ishizuka, F. Tsuboi, K. Tsuchiya, Development of an electrostatic generator that harnesses the motion of a living body: use of a resonant phenomenon, JSME International Journal Series C Mechanical Systems, Machine Elements and Manufacturing 43(4) (2000) 916-922.
[10] H. Xue, Q. Yang, D. Wang, W. Luo, W. Wang, M. Lin, D. Liang, Q. Luo, A wearable pyroelectric nanogenerator and self-powered breathing sensor, Nano Energy 38 (2017) 147-154.
[11] H. Kulah, K. Najafi, An electromagnetic micro power generator for low-frequency environmental vibrations, 17th IEEE International Conference on Micro Electro Mechanical Systems. Maastricht MEMS 2004 Technical Digest, IEEE, 2004, pp. 237-240.

[12] P. Niu, P. Chapman, R. Riemer, X. Zhang, Evaluation of motions and actuation methods for biomechanical energy harvesting, 2004 IEEE 35th annual power electronics specialists conference (IEEE Cat. No. 04CH37551), IEEE, 2004, pp. 2100-2106.
[13] M.M. Alam, A. Sultana, D. Mandal, Biomechanical and acoustic energy harvesting from TiO2 nanoparticle modulated PVDF nanofiber made high performance nanogenerator, ACS Applied Energy Materials 1(7) (2018) 3103-3112.
[14] A. Sultana, M.M. Alam, S.K. Ghosh, T.R. Middya, D. Mandal, Energy harvesting and self-powered microphone application on multifunctional inorganic-organic hybrid nanogenerator, Energy 166 (2019) 963-971.
[15] M.A. Johar, J.-H. Kang, M.A. Hassan, S.-W. Ryu, A scalable, flexible and transparent GaN based heterojunction piezoelectric nanogenerator for bending, air-flow and vibration energy harvesting, Applied energy 222 (2018) 781-789.
[16] A.M. Abdullah, M.U.K. Sadaf, F. Tasnim, H. Vasquez, K. Lozano, M.J. Uddin, KNN based piezo-triboelectric lead-free hybrid energy films, Nano Energy 86 (2021) 106133.
[17] S.M.A.Z. Shawon, A.X. Sun, V.S. Vega, B.D. Chowdhury, P. Tran, Z.D. Carballo, J.A. Tolentino, J. Li, M.S. Rafaqut, S. Danti, Piezo-Tribo Dual Effect Hybrid Nanogenerators for Health Monitoring, Nano Energy (2020) 105691.
[18] X. Cheng, X. Xue, Y. Ma, M. Han, W. Zhang, Z. Xu, H. Zhang, H. Zhang, Implantable and self-powered blood pressure monitoring based on a piezoelectric thinfilm: Simulated, in vitro and in vivo studies, Nano Energy 22 (2016) 453-460.
[19] R. Van Schaijk, R. Elfrink, J. Oudenhoven, V. Pop, Z. Wang, M. Renaud, A MEMS vibration energy harvester for automotive applications, Smart Sensors, Actuators, and MEMS VI, International Society for Optics and Photonics, 2013, p. 876305.
[20] D. Zhu, S.P. Beeby, M.J. Tudor, N.R. Harris, A credit card sized self powered smart sensor node, Sensors and Actuators A: Physical 169(2) (2011) 317-325.
[21] Z.L. Wang, J. Song, Piezoelectric nanogenerators based on zinc oxide nanowire arrays, Science 312(5771) (2006) 242-246.
[22] R. Wang, S. Liu, C.R. Liu, W. Wu, Data-driven learning of process− property− performance relation in laser-induced aqueous manufacturing and integration of ZnO piezoelectric nanogenerator for self-powered nanosensors, Nano Energy 83 (2021) 105820.
[23] D.-C. Yang, Y. Qiu, Q.-Y. Jiang, Z.-S. Guo, Paper Fiber Paper-Based ZnO Piezoelectric Nanogenerator for Self-Powered Energy Scavenging, Materials in Environmental Engineering, De Gruyter2017, pp. 705-714.
[24] H. Liu, J. Zhong, C. Lee, S.-W. Lee, L. Lin, A comprehensive review on piezoelectric energy harvesting technology: Materials, mechanisms, and applications, Applied Physics Reviews 5(4) (2018) 041306.
[25] G.T. Hwang, V. Annapureddy, J.H. Han, D.J. Joe, C. Baek, D.Y. Park, D.H. Kim, J.H. Park, C.K. Jeong, K.I. Park, Self - powered wireless sensor node enabled by an aerosol - deposited PZT flexible energy harvester, Advanced Energy Materials 6(13) (2016) 1600237.
[26] R. Guo, Y. Guo, H. Duan, H. Li, H. Liu, Synthesis of orthorhombic perovskite-type ZnSnO3 single-crystal nanoplates and their application in energy harvesting, ACS applied materials & interfaces 9(9) (2017) 8271-8279.
[27] S.K. Karan, R. Bera, S. Paria, A.K. Das, S. Maiti, A. Maitra, B.B. Khatua, An Approach to Design Highly Durable Piezoelectric Nanogenerator Based on Self-Poled PVDF/AlO-rGO Flexible Nanocomposite with High Power Density and Energy Conversion Efficiency, Advanced Energy Materials 6(20) (2016) 1601016.
[28] A. Biswas, S. Saha, N.R. Jana, ZnSnO3 nanoparticle-based piezocatalysts for ultrasound-assisted degradation of organic pollutants, ACS Applied Nano Materials 2(2) (2019) 1120-1128.
[29] J. Zhu, H. Li, L. Zhong, P. Xiao, X. Xu, X. Yang, Z. Zhao, J. Li, Perovskite oxides: preparation, characterizations, and applications in heterogeneous catalysis, Acs Catalysis 4(9) (2014) 2917-2940.

[30] C. Baek, J.E. Wang, S. Ryu, J.-H. Kim, C.K. Jeong, K.-I. Park, D.K. Kim, Facile hydrothermal synthesis of BaZrxTi1−xO3 nanoparticles and their application to a lead-free nanocomposite generator, RSC Advances 7(5) (2017) 2851 - 2856.
[31] Y. Zhang, H. Kim, Q. Wang, W. Jo, A.I. Kingon, S.-H. Kim, C.K. Jeong, Progress in lead-free piezoelectric nanofiller materials and related composite nanogenerator devices, Nanoscale Advances 2(8) (2020) 3131-3149.
[32] K.Y. Lee, D. Kim, J.H. Lee, T.Y. Kim, M.K. Gupta, S.W. Kim, Unidirectional high - power generation via stress - induced dipole alignment from ZnSnO3 nanocubes/polymer hybrid piezoelectric nanogenerator, Advanced Functional Materials 24(1) (2014) 37-43.
[33] M.M. Alam, S.K. Ghosh, A. Sultana, D. Mandal, Lead-free ZnSnO3/MWCNTs-based self-poled flexible hybrid nanogenerator for piezoelectric power generation, Nanotechnology 26(16) (2015) 165403.
[34] J. Xu, X. Jia, X. Lou, J. Shen, One-step hydrothermal synthesis and gas sensing property of ZnSnO3 microparticles, Solid-State Electronics 50(3) (2006) 504-507.
[35] A. Rovisco, A. dos Santos, T. Cramer, J. Martins, R. Branquinho, H. Águas, B. Fraboni, E. Fortunato, R. Martins, R. Igreja, Piezoelectricity Enhancement of Nanogenerators Based on PDMS and ZnSnO3 Nanowires through Microstructuration, ACS Applied Materials & Interfaces 12(16) (2020) 18421-18430.
[36] J.M. Wu, C. Xu, Y. Zhang, Y. Yang, Y. Zhou, Z.L. Wang, Flexible and Transparent Nanogenerators Based on a Composite of Lead-Free ZnSnO3 Triangular-Belts, Adv. Mater. (Weinheim, Ger.) 24(45) (2012) 6094-6099.
[37] J.M. Wu, C. Xu, Y. Zhang, Z.L. Wang, Lead-free nanogenerator made from single ZnSnO3 microbelt, ACS nano 6(5) (2012) 4335-4340.
[38] S. Paria, S. Ojha, S.K. Karan, S.K. Si, R. Bera, A.K. Das, A. Maitra, L. Halder, A. De, B.B. Khatua, Approach for enhancement in output performance of randomly oriented ZnSnO3 nanorod-based piezoelectric nanogenerator via p-n heterojunction and surface passivation layer, ACS Appl. Electron. Mater. 2(8) (2020) 2565-2578.
[39] R. Guo, Y. Guo, H. Duan, H. Li, H. Liu, Synthesis of Orthorhombic Perovskite-Type ZnSnO3 Single-Crystal Nanoplates and Their Application in Energy Harvesting, ACS Appl. Mater. Interfaces 9(9) (2017) 8271-8279.
[40] G. Wang, Y. Xi, H. Xuan, R. Liu, X. Chen, L. Cheng, Hybrid nanogenerators based on triboelectrification of a dielectric composite made of lead-free ZnSnO3 nanocubes, Nano Energy 18 (2015) 28-36.
[41] M.M. Alam, S.K. Ghosh, A. Sultana, D. Mandal, Lead-free ZnSnO3/MWCNTs-based selfpoled flexible hybrid nanogenerator for piezoelectric power generation, Nanotechnology 26(16) (2015) 1-6.
[42] S. Paria, S.K. Karan, R. Bera, A.K. Das, A. Maitra, B.B. Khatua, A facile approach to develop a highly stretchable PVC/ZnSnO3 piezoelectric nanogenerator with high output power generation for powering portable electronic devices, Industrial & Engineering Chemistry Research 55(40) (2016) 10671-10680.
[43] Z. Wang, J. Liu, F. Wang, S. Chen, H. Luo, X. Yu, Size-Controlled Synthesis of ZnSnO3 Cubic Crystallites at Low Temperatures and Their HCHO-Sensing Properties, The Journal of Physical Chemistry C 114(32) (2010) 13577-13582.
[44] S. Lee, J. Lee, W. Ko, S. Cha, J. Sohn, J. Kim, J. Park, Y. Park, J. Hong, Solution-processed Ag-doped ZnO nanowires grown on flexible polyester for nanogenerator applications, Nanoscale 5(20) (2013) 9609-9614.
[45] C. Liu, A. Yu, M. Peng, M. Song, W. Liu, Y. Zhang, J. Zhai, Improvement in the piezoelectric performance of a ZnO nanogenerator by a combination of chemical doping and interfacial modification, The Journal of Physical Chemistry C 120(13) (2016) 6971-6977.
[46] S. Lu, Q. Liao, J. Qi, S. Liu, Y. Liu, Q. Liang, G. Zhang, Y. Zhang, The enhanced performance of piezoelectric nanogenerator via suppressing screening effect with Au particles/ZnO nanoarrays Schottky junction, Nano Research 9(2) (2016) 372-379.

[47] S. Paria, S. Ojha, S.K. Karan, S.K. Si, R. Bera, A.K. Das, A. Maitra, L. Halder, A. De, B.B. Khatua, Approach for Enhancement in Output Performance of Randomly Oriented ZnSnO3 Nanorod-Based Piezoelectric Nanogenerator via p–n Heterojunction and Surface Passivation Layer, ACS Applied Electronic Materials 2(8) (2020) 2565-2578.
[48] A. Rovisco, A. Dos Santos, T. Cramer, J. Martins, R. Branquinho, H. Águas, B. Fraboni, E. Fortunato, R. Martins, R. Igreja, Piezoelectricity enhancement of nanogenerators based on PDMS and ZnSnO3 nanowires through microstructuration, ACS applied materials & interfaces 12(16) (2020) 18421-18430.
[49] B. Dudem, L.K. Bharat, H. Patnam, A.R. Mule, J.S. Yu, Enhancing the output performance of hybrid nanogenerators based on Al-doped BaTiO 3 composite films: a self-powered utility system for portable electronics, Journal of Materials Chemistry A 6(33) (2018) 16101-16110.
[50] D. Xu, W. Li, L. Wang, W. Wang, W. Cao, W. Fei, Large piezoelectric properties induced by doping ionic pairs in BaTiO3 ceramics, Acta materialia 79 (2014) 84-92.
[51] S.S.H. Abir, S.K. Gupta, A. Ibrahim, B.B. Srivastava, K. Lozano, Tunable CsPb (Br/Cl) 3 perovskite nanocrystals and further advancement in designing light emitting fiber membranes, Materials Advances 2(8) (2021) 2700-2710.
[52] Z. Wang, J. Liu, F. Wang, S. Chen, H. Luo, X. Yu, Size-controlled synthesis of ZnSnO3 cubic crystallites at low temperatures and their HCHO-sensing properties, The Journal of Physical Chemistry C 114(32) (2010) 13577-13582.
[53] H. Park, D.Y. Hyeon, M. Jung, K.-I. Park, J. Park, Piezoelectric BaTiO3 microclusters and embossed ZnSnO3 microspheres-based monolayer for highly-efficient and flexible composite generator, Composites Part B: Engineering 203 (2020) 108476.
[54] G. Suo, Y. Yu, Z. Zhang, S. Wang, P. Zhao, J. Li, X. Wang, Piezoelectric and triboelectric dual effects in mechanical-energy harvesting using BaTiO3/polydimethylsiloxane composite film, ACS applied materials & interfaces 8(50) (2016) 34335-34341.
[55] N.P.M.J. Raj, N.R. Alluri, G. Khandelwal, S.-J. Kim, Lead-free piezoelectric nanogenerator using lightweight composite films for harnessing biomechanical energy, Composites Part B: Engineering 161 (2019) 608-616.
[56] H. Wang, H. Huang, B. Wang, First-principles study of structural, electronic, and optical properties of ZnSnO3, Solid state communications 149(41-42) (2009) 1849-1852.
[57] L. Jin, S. Ma, W. Deng, C. Yan, T. Yang, X. Chu, G. Tian, D. Xiong, J. Lu, W. Yang, Polarization-free high-crystallization β-PVDF piezoelectric nanogenerator toward self-powered 3D acceleration sensor, Nano Energy 50 (2018) 632-638.
[58] J. Briscoe, S. Dunn, Piezoelectric nanogenerators–a review of nanostructured piezoelectric energy harvesters, Nano Energy 14 (2015) 15-29.
[59] H. Mizoguchi, P.M. Woodward, Electronic structure studies of main group oxides possessing edge-sharing octahedra: implications for the design of transparent conducting oxides, Chemistry of materials 16(25) (2004) 5233-5248.
[60] J. Phillips, Bonds and Bands in Semiconductors (Acade, Press, New York (1973).
[61] T. Minami, H. Sonohara, S. Takata, H. Sato, Highly transparent and conductive zinc-stannate thin films prepared by RF magnetron sputtering, Japanese journal of applied physics 33(12A) (1994) L1693.
[62] K. Chopra, S. Major, D. Pandya, Transparent conductors—a status review, Thin solid films 102(1) (1983) 1-46.
[63] H. Iida, N. Shiba, T. Mishuku, H. Karasawa, A. Ito, M. Yamanaka, Y. Hayashi, Efficiency of the a-Si: H solar cell and grain size of SnO 2 transparent conductive film, IEEE Electron Device Letters 4(5) (1983) 157-159.
[64] A.R. Chowdhury, A.M. Abdullah, I. Hussain, J. Lopez, D. Cantu, S.K. Gupta, Y. Mao, S. Danti, M.J. Uddin, Lithium doped zinc oxide based flexible piezoelectric-triboelectric hybrid nanogenerator, Nano Energy 61 (2019) 327-336.

[65] A.R. Chowdhury, A.M. Abdullah, U.V. Romero, I. Hussain, C. Olivares, S. Danti, J. Li, M.J. Uddin, Decentralized triboelectric electronic health monitoring flexible microdevice, Medical Devices & Sensors 3(6) (2020) e10103.
[66] A.M. Abdullah, A. Flores, A.R. Chowdhury, J. Li, Y. Mao, M.J. Uddin, Synthesis and fabrication of self-sustainable triboelectric energy case for powering smart electronic devices Nano Energy 73 (2020) 104774.
[67] V. Vivekananthan, A. Chandrasekhar, N.R. Alluri, Y. Purusothaman, W.J. Kim, C.-N. Kang, S.-J. Kim, A flexible piezoelectric composite nanogenerator based on doping enhanced lead-free nanoparticles, Materials Letters 249 (2019) 73-76.
[68] Y. Zhang, M. Wu, Q. Zhu, F. Wang, H. Su, H. Li, C. Diao, H. Zheng, Y. Wu, Z.L. Wang, Performance enhancement of flexible piezoelectric nanogenerator via doping and rational 3D structure design for self - powered mechanosensational system, Advanced Functional Materials 29(42) (2019) 1904259.
[69] S.-H. Shin, Y.-H. Kim, M.H. Lee, J.-Y. Jung, J.H. Seol, J. Nah, Lithium-doped zinc oxide nanowires–polymer composite for high performance flexible piezoelectric nanogenerator, ACS nano 8(10) (2014) 10844-10850.
[70] M. Manikandan, P. Rajagopalan, N. Patra, S. Jayachandran, M. Muralidharan, S.M. Prabu, I. Palani, V. Singh, Development of Sn-doped ZnO based ecofriendly piezoelectric nanogenerator for energy harvesting application, Nanotechnology 31(18) (2020) 185401.
[71] H. Parangusan, D. Ponnamma, M.A.A. AlMaadeed, Flexible tri-layer piezoelectric nanogenerator based on PVDF-HFP/Ni-doped ZnO nanocomposites, RSC advances 7(79) (2017) 50156-50165.
[72] A.R. Chowdhury, A.M. Abdullah, I. Hussain, J. Lopez, D. Cantu, S.K. Gupta, Y. Mao, S. Danti, M.J. Uddin, Lithium doped zinc oxide based flexible piezoelectric-triboelectric hybrid nanogenerator, Nano Energy 61 (2019) 327-336.
[73] C. Chang, V.H. Tran, J. Wang, Y.-K. Fuh, L. Lin, Direct-write piezoelectric polymeric nanogenerator with high energy conversion efficiency, Nano Letters 10(2) (2010) 726-731.
[74] L. Gu, N. Cui, L. Cheng, Q. Xu, S. Bai, M. Yuan, W. Wu, J. Liu, Y. Zhao, F. Ma, Flexible fiber nanogenerator with 209 V output voltage directly powers a light-emitting diode, Nano Letters 13(1) (2013) 91-94.
[75] M.-L. Seol, H. Im, D.-I. Moon, J.-H. Woo, D. Kim, S.-J. Choi, Y.-K. Choi, Design strategy for a piezoelectric nanogenerator with a well-ordered nanoshell array, ACS nano 7(12) (2013) 10773-10779.
[76] S. Siddiqui, D.-I. Kim, M.T. Nguyen, S. Muhammad, W.-S. Yoon, N.-E. Lee, High-performance flexible lead-free nanocomposite piezoelectric nanogenerator for biomechanical energy harvesting and storage, Nano Energy 15 (2015).
[77] X. Xia, J. Chen, G. Liu, M.S. Javed, X. Wang, C. Hu, Aligning graphene sheets in PDMS for improving output performance of triboelectric nanogenerator, Carbon 111 (2017) 569-576.
[78] B. Dudem, N.D. Huynh, W. Kim, D.H. Kim, H.J. Hwang, D. Choi, J.S. Yu, Nanopillar-array architectured PDMS-based triboelectric nanogenerator integrated with a windmill model for effective wind energy harvesting, Nano Energy 42 (2017) 269-281.
[79] J. Chen, H. Guo, X. He, G. Liu, Y. Xi, H. Shi, C. Hu, Enhancing performance of triboelectric nanogenerator by filling high dielectric nanoparticles into sponge PDMS film, ACS Aplied Materials & Interfaces 8(1) (2016) 736-744.
[80] Y. Yang, H. Zhang, Z.-H. Lin, Y.S. Zhou, Q. Jing, Y. Su, J. Yang, J. Chen, C. Hu, Z.L. Wang, Human skin based triboelectric nanogenerators for harvesting biomechanical energy and as self-powered active tactile sensor system, ACS nano 7(10) (2013) 9213-9222.
[81] C. Peters, J. Handwerker, D. Maurath, Y. Manoli, An ultra-low-voltage active rectifier for energy harvesting applications, Proceedings of 2010 IEEE International Symposium on Circuits and Systems, IEEE, 2010, pp. 889-892.

[82] S. Bhunia, S. Chandel, S.K. Karan, S. Dey, A. Tiwari, S. Das, N. Kumar, R. Chowdhury, S. Mondal, I. Ghosh, A. Mondal, B.B. Khatua, N. Ghosh, C.M. Reddy, Autonomous self-repair in piezoelectric molecular crystals, Science 373(6552) (2021) 321-327.

Author Biography:

Sk Md Ali Zaker Shawon received his B.Sc. in Chemical Engineering from Jashore University of Science and Technology, Bangladesh in 2013. Then he joined as a "Process Engineer" in one of the biggest petrochemical companies in Bangladesh. He joined Photonics and Energy Research Laboratory at the University of Texas Rio Grande Valley in 2019 as a graduate student. His research interests include the application of nanostructured functional interfaces in hybrid nanogenerators, the development of antimicrobial and antiviral textile fibers, dye-sensitized solar cells, renewable energy, and electromechanical sensors. Sk Md Ali Zaker Shawon is recently awarded: Presidential Graduate Research Fellowship (2019- 2021), HSS Competition Award (2nd Prize-Co mentor).

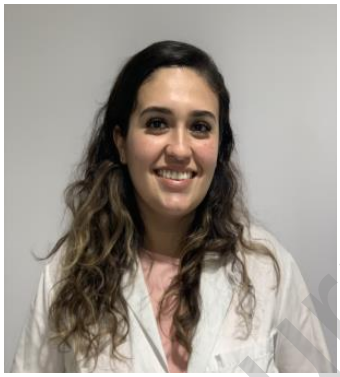

Valeria Suarez Vega received her B. Sc. in Biochemistry from Sonoma State University, United States in 2019. She joined the Photonics and Energy Research Laboratory at the University of Texas Rio Grande Valley in 2020 as a graduate student. Her research interests are the development of multifunctional antimicrobial and antiviral textiles and the application of functional interfaces in hybrid nanogenerators. Valeria Suarez Vega is recently awarded: Presidential Graduate Research Fellowship (2020-2022).

Dr. Jianzhi (James) Li received Ph.D. in Industrial Engineering from Texas Tech University, Lubbock, in 2003. Currently, Dr. Li is a Professor of Manufacturing Engineering, and Olegario Vazquez Rana Endowed Fellow at The University of Texas, Rio Grande Valley. His professional experiences also include working as product engineer in the automobile industry and serving as technical director in the information technology and logistics fields. His research has focused on additive manufacturing, laser material processing, optimization, and sustainable manufacturing. His current research topics also include bio printing for tissue regeneration and STEM education. He received grants from various sources including federal government agencies and industries. He is currently leading a grant

from DoD Manufacturing Technology (MTech) Program with a goal to develop a national consortium (I-DREAM4D) to support research and education in Advanced Manufacturing for the defense.

Dr. M. Jasim Uddin (h-index 30, Associate Professor) obtained his Ph.D. degree (Materials Science) from the University of Turin, Italy. He is currently holding interim-chair position of department chair of the Department of Chemistry and Director of Photonics and Energy Research Laboratory (PERL) in the Department of Chemistry, University of Texas Rio Grande Valley. He worked at Tulane University, LA, and Florida State University, FL. He is known for the invention of three-dimensional solar cells, and self-cleaning, antimicrobial textiles, and photochromic textiles. He is recently awarded: High Scholar Research Competition Award 2016, 2018, & 2020 (UTRGV), Outstanding and Sustainable Research in Science Award 2016 (UTRGV), United Group Research Award 2016 (International), NASA Texas Space Grant Award (2016), UGC Award in 2010 (International), etc.

CRediT authorship contribution statement

Sk Md Ali Zaker Shawon: Conceptualization, Methodology, Investigation, Data Curation, Writing– Original Draft, Writing- Review & Editing.
Zaida D. Carballo: Investigation, Data Curation, Writing – Original Draft, Writing- Review & Editing.
Valeria Suarez Vega: Methodology, Investigation, Data Curation, Writing- Review & Editing.
Chen Lin: Methodology, Investigation, Data Curation, Writing- Review & Editing.
Muhammad Sufian Rafaqut: Data Curation, Visualization.
Andrew Xu Sun: Investigation, Writing- Original Draft.
James Li: Writing- Review & Editing, Funding acquisition, Supervision, Project administration.
M. Jasim Uddin: Writing – Original Draft, Writing- Review & Editing, Funding acquisition, Supervision, Project administration.

Highlights

- Surface modified Al doped ZnSnO3 PENG for enhanced piezoelectric power generation
- Low temperature solution method was introduced to synthesize ZnSnO3 nanocubes of particle size 30nm-55nm.
- The as synthesized highly efficient PENG was installed in a helmet
- The ability of this helmet to detect human movement and transmit them wirelessly as a motion sensor transmutes it into a smart helmet.